Applied Thermal Engineering 225 (2023) 120157

Contents lists available at ScienceDirect

Applied Thermal Engineering

journal homepage: www.elsevier.com/locate/apthermeng

Research Paper

A novel nonlinear radiative heat exchanger for molten-salt applications

Z. Li [a], N. Le Brun [a], C. Gasparrini [b], C.N. Markides [a,*]

[a] Clean Energy Processes (CEP) Laboratory, Department of Chemical Engineering, Imperial College London, London SW7 2AZ, United Kingdom
[b] Centre for Nuclear Engineering (CNE) & Department of Materials, Imperial College London, London SW7 2AZ, United Kingdom

ARTICLE INFO

Keywords:
DRACS
Freezing
Heat exchanger
Molten salt
MSR

ABSTRACT

One of the main difficulties associated with using molten salts as heat transfer fluids (HTFs) in practical applications such as in the solar and nuclear energy industries is the possibility of solidifying molten salts. Since the salts proposed for Generation-IV nuclear reactors (MSRs) have higher melting points, this is especially true for those reactors. The consequences of accidental freezing within the direct reactor auxiliary cooling system (DRACS) of MSRs could be catastrophic. DRACS is a passive safety system designed to remove decay heat from the reactor core during an emergency. The present study examines, as a case study, the freezing problem in the most vulnerable component of DRACS, namely the natural draft heat exchanger (NDHX). For this application, a unique and innovative heat exchanger design termed radiative heat exchanger (RHX) is proposed, with nonlinear heat transfer characteristics. Specifically, by suppressing convection and exploiting thermal radiation as the primary heat transfer mechanism, the RHX concept reduces the heat rejection/removal rate passively to allow safe operation when the molten salt coolant temperature drops and is near its melting point, while maintaining a high capacity for decay heat extraction in case the coolant temperature rises during an accident and the reactor becomes overheated; this moderation of the heat removal rate is accomplished without the requirement for external (manual or automatic) control. A thermohydraulic model is developed and applied to evaluate the proposed RHX with the existing conventional NDHX. Compared to the conventional design, the RHX has the potential to reduce heat removal by approximately 30 % at low temperatures and near-solidification conditions. In the case of the prototypical 20 MW reactor with a decay rate of 0.2 MW, RHX extends the freezing time of molten salt by three times, to approximately 18 h. During high-temperature events, such as the initial stages of a reactor scram, the RHX can improve decay heat extraction by 17 %. Other applications of molten salts with similar challenges can also be addressed using the proposed design approach.

Nomenclature

A	Surface area [m^2]
D	Outside diagram of heat-exchanger tube [m]
F	View factor [-]
Gr	Grashof number [-]
L	Length [m]
Nu	Nusselt number [-]
Pr	Prandtl number [-]
Re	Reynolds number [-]
T	Temperature [K]
Q	Heat flow rate, thermal power [W]
c_p	Specific heat capacity [J kg^{-1} K^{-1}]
f	Friction factor [-]
g	Gravitational acceleration [m s^{-2}]
h	Heat transfer coefficient [W m^{-2} K^{-1}]
k	Thermal conductivity [W m^{-1} K^{-1}]

(*continued on next column*)

Nomenclature (*continued*)

r	Radius [m]
Greek symbol	
ε	Emissivity [-]
μ	Dynamic (absolute) viscosity [kg m^{-1} s^{-1}]
ρ	Density [kg m^{-3}]
σ	Stefan-Boltzmann constant [-]
Subscript	
air	Ambient air
in	Internal side
salt	Salt
out	External side
s	Steady state
Abbreviations	
ARE	Aircraft reactor experiment
DHX	Dracs heat exchanger
DRACS	Direct reactor auxiliary cooling system

(*continued on next page*)

* Corresponding author.
E-mail address: cep-lab@imperial.ac.uk (C.N. Markides).

https://doi.org/10.1016/j.applthermaleng.2023.120157
Received 28 June 2022; Received in revised form 3 November 2022; Accepted 31 January 2023
Available online 4 February 2023

Nomenclature (*continued*)

HTC	Heat transfer coefficient
ID	Inside diameter
LOFC	Loss of forces circulation
LWR	Light water reactor
MSR	Molten salt reactor
MSRE	Molten salt reactor experiment
NDHX	Natural draft heat exchanger
ORNL	Oak Ridge National Laboratory
OD	Outside diameter
RHX	Radiative heat exchanger
SHX	Standard heat exchanger

1. Introduction

Molten salt technology has been studied extensively in recent years and is increasingly being utilised in energy fields such as solar power generation [1–3] and thermal energy storage [4,5]. This interest has resulted from the favourable physicochemical properties of molten salts relative to conventional heat transfer fluids (HTFs), such as their large specific heat capacities, good thermal conductivities [6–8], high boiling points at near-atmospheric pressures, and lower vapour pressures, but also their superior chemical stability, irradiation resistance and relative cost-effectiveness [9–11]. Thanks to these superior properties and characteristics, molten salts are being considered next-generation HTFs and thermal storage materials for high-temperature applications, particularly in the nuclear energy sector [12–15].

Research on molten salts as HTFs for nuclear applications started in the 1950 s with the U.S. Aircraft Reactor Experiment (ARE), a 2.5 MW nuclear reactor experiment aimed at attaining a nuclear engine for aircraft propulsion [16,17]. In the 1960 s, Oak Ridge National Laboratory (ORNL) took the lead in researching MSRs and their work culminated with a 7.4 MW test reactor named Molten-Salt Reactor Experiment (MSRE) [18]. From 1970 to 1976, ORNL designed a molten-salt breeder reactor (MSBR) with a 705 °C peak operating temperature. However, following this development, the MSR program in the U.S. was abandoned in favour of liquid–metal fast reactors [19]. During the same period, the U.K.'s Atomic Energy Research Establishment (AERE) proceeded with the development of an alternative 2.5 MW molten-salt fast reactor (MSFR) concept fuelled by plutonium; unfortunately, this program similarly came to an end, before its completion, in 1974 [20].

Recently, interest in MSRs in both solar and nuclear applications has reignited. In the nuclear industry, MSRs are considered a promising alternative to conventional light-water reactors (LWRs) due to their inherent safety features [21], and their design is regarded as one of the most sustainable nuclear fission reactor concepts [22]. The most significant advantage of MSRs compared to LWRs is that MSRs can operate at higher critical temperatures over wider temperature excursions. This advantage derives from the high boiling point of molten salts and their chemical stability under irradiation. MSRs are capable of operating at temperatures up to 1400 °C, close to atmospheric pressure. Pressurised-water reactors (PWRs), which account for the majority of the world's LWR fleet, use high-pressure water as the HTF (at around 150 bar) and are therefore limited to operation at temperatures below 350 °C. Operating a reactor at a higher temperature, which is possible for MSRs, can enhance the power conversion efficiency and considerably reduce fissile fuel consumption [23]. Moreover, MSRs are associated with an additional inherent safety feature as they can operate with little or no pressurisation. Low operating pressures essentially reduce the risk of structural failure (*e.g.*, pipe rupture) and loss of coolant accident (LOCA) scenarios. In addition, operation at low pressure allows the walls of the reactor vessel and pipelines to be thinner, simplifying the design and considerably reducing costs.

On the other hand, some of the drawbacks of using molten salts as HTFs are related to the possible deterioration of the structural materials used, caused by corrosion and irradiation embrittlement [24–27]. Additionally, due to the high melting points of suitable molten salts, accidental solidification could be an issue that prevents their use in this application. This issue has been encountered in the solar industry, which has resulted in complications (*e.g.*, the receiver tube may rupture or experience substantially reduced life expectancy) [28,29] and the need for innovative freeze protection solutions [12]. The same phenomenon in the nuclear sector is even more challenging as the molten salts being considered for MSRs have higher melting points [30]. For instance, the melting point of chloride and fluoride eutectics, one of the most promising molten salts in the nuclear industry, is generally > 450 °C (those adopted in solar applications are around 150 °C).

The accidental solidification of the coolant induces two adverse effects in MSRs: (1) coolant can damage the pipes through stresses generated by the volumetric expansion associated with the phase transition; and (2) solidification can partially or even entirely clog the pipelines of coolant loops impeding fluid circulation and heat dissipation. The phenomenon of fluid circulation obstruction induced by clogging drastically reduces the cooling efficiency and can even completely block coolant flow in the extreme [31,32].

The issue of coolant freezing in MSRs was recognised at the research stages of the MSRE by ORNL in the 1960s. As a precaution against this hazard, sets of electric heaters were installed in every salt-containing component of the MSRE to maintain the coolant temperature above the melting point [33]; this solution is also nowadays commonly implemented in the concentrated solar power (CSP) industry [34]. In addition to this engineering solution, quick-closing doors and an independent cooling device referred to as a 'radiator' were installed. These doors were designed to prevent salt freezing in the radiator tubes by providing quick air shutoff [33]. Unfortunately, these measures all depend on the availability of an external power supply and control systems, which cannot always be guaranteed, especially in the event of accidents, such as the one at Fukushima Daiichi [35].

In an effort to mitigate the consequences of accidental salt solidification, this study aims to develop a reliable safety function that does not require external power supply or active control. As part of this effort, also as a case study, the study examines the freezing problem of molten salts in the direct reactor auxiliary cooling system (DRACS), shown in Fig. 1. In an emergency scenario of loss of forced circulation (LOFC), *e.g.*, such as at Fukushima Daiichi, a safety system is required that is capable of removing decay heat from the reactor core passively via natural circulation [36], while alleviating the risks that arise due to salt solidification at lower temperatures. Considering the enormous heat generated by decay (7 % of the reactor's generating capacity [37]) and the fact that this heat is exclusively removed by DRACS, the consequences of DRACS failure can be catastrophic [38,39]. For example, DRACS failure caused by clogging of solidified coolants can bring the reactor temperature up to 900 °C within 4 h [21].

As shown in Fig. 1, DRACS is composed of two interconnected, primary and secondary, natural circulation loops, within which molten salts flow and exchange heat through the DRACS heat exchanger (DHX). A fluid diode inhibits molten salt circulation in both loops in non-emergency situations to prevent excessive thermal loss, thereby keeping the salt from solidifying. Nevertheless, in a reactor scram, an air inlet is opened in the secondary loop chimney, allowing natural circulation in both loops due to the thermal gradient, allowing decay heat to be removed by molten salt/air heat exchangers in the secondary loop, also known as natural draft heat exchangers (NDHX).

Due to its location far from the reactor core and exposure to the environment, the NDHX is the most vulnerable unit in the DRACS since the coolant is at its lowest temperature. The conventional NDHX designs covered in the literature do not address the hazards that arises due to the coolant solidification, which can allow the reactor to reach dangerous operating conditions [21]. Therefore, the present study proposes a unique and innovative design approach for the NDHX, which promotes thermal radiation as the primary heat transfer mechanism by

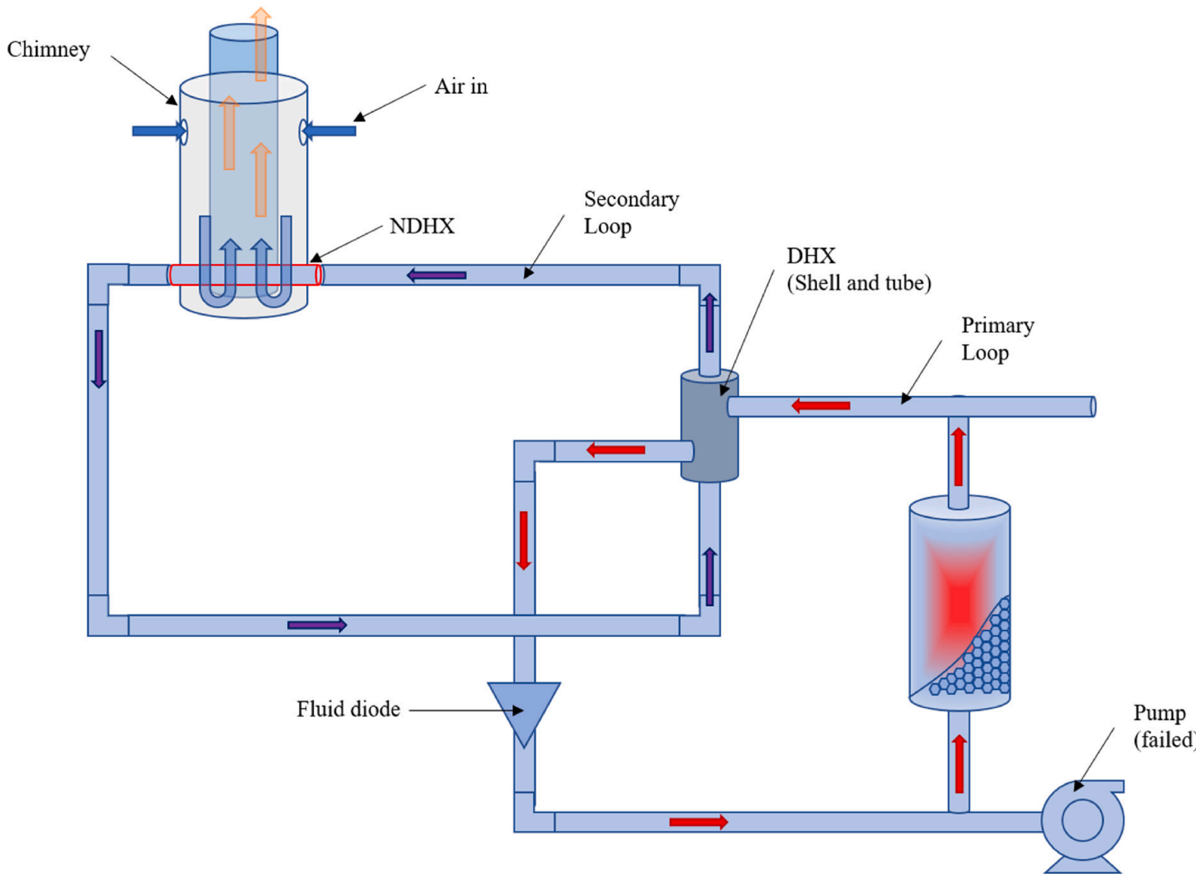

Fig. 1. Simplified schematic of DRACS during LOFC. In the primary loop, the anticlockwise direction (red arrows) indicates the preferred direction of the fluidic diode, which is the coolant (*i.e.*, molten salt) flow direction during the emergency. With the primary coolant flowing into the DHX and rejecting heat into the secondary loop, the circulation of the secondary coolant is then initialised (purple arrows). Ultimately, all the heat will be extracted by the NDHX [21]. (For interpretation of the references to colour in this figure legend, the reader is referred to the web version of this article.)

suppressing convective heat transfer, termed 'radiative heat exchanger' (RHX). Such a heat exchanger takes advantage of thermal radiation's inherent and strongly nonlinear properties, passively reduces the heat rejection/removal rate at lower temperatures, and suppresses the risk of solidification. This innovative heat exchanger design concept has the potential to avoid or mitigate salt solidification at lower temperatures, while effectively removing decay heat at higher temperatures. To the best knowledge of the authors, this is the first time that such a design has been proposed and studied to address the issue of salt solidification. The operating performance of a RHX design is assessed using an in-house thermohydraulic model developed for this study, which is also capable of predicting coolant freezing or performing analyses of this heat exchanger's performance.

This paper consists of five sections, including this introductory section. As part of Section 2, detailed annotations are provided for the conventional NDHX design, referred to as a 'standard heat exchanger' (abbreviated SHX to differentiate it from the RHX), and the novel RHX design. Section 3 provides a description of the modelling and evaluation methods. The results of the simulations are presented in Section 4, along with detailed evaluations of two designs under various what-if scenarios. The main conclusions are summarised in Section 5.

2. Conventional and novel natural draft heat exchanger

2.1. Layout of conventional natural draft heat exchanger

As described in the previous section, the NDHX is a molten salt-air heat exchanger, wherein ambient air and molten salt coolant circulate naturally, driven by temperature differences. In a conventional NDHX design (see Fig. 2), the molten-salt coolant, assumed here to be FLiNaK (LiF–NaF–KF: 29–12–59 wt%), flows into a straight tube bundle arranged in layers of parallel tubes. The ambient air flows over the external surface of the tube bundle, as illustrated in Fig. 2. In order to improve the natural draft circulation of the airflow, the heat exchanger is placed at the bottom of a chimney outside the reactor building. Ambient air enters the chimney from the bottom via louvres, which can be adjusted to control the airflow and, therefore, the total heat rejection capability of the DRACS. As a safety measure, the louvres are entirely opened in the event of a blackout, preventing any flow obstruction. A configuration with fully opened louvres is assumed in the current study to analyse severe emergencies such as a complete loss of external power supply, similar to the Fukushima Daiichi accident.

The design and main geometrical parameters of the conventional NDHX adopted in this work were taken as a reference from Ref. [39]. This prototypic DRACS design has the capacity to remove 0.2 MW of decay heat from a 20 MW fluoride salt-cooled high-temperature reactor (FHR), or roughly 1 % of the operational reactor power. The NDHX design adopted is termed the 'standard heat exchanger' (SHX) to distinguish it from the 'radiative heat exchanger' (RHX) design proposed and investigated in the present work. The SHX comprises two rows of tubes, each with fifty tubes placed horizontally, one on top of the other in the air chimney, as shown in Fig. 3. Each individual tube has an inner diameter of 13.3 mm, an outer diameter of 15.9 mm and a total length of 1.93 m. The chimney is set to be 10 m tall with a cross-sectional area of 4 m^2.

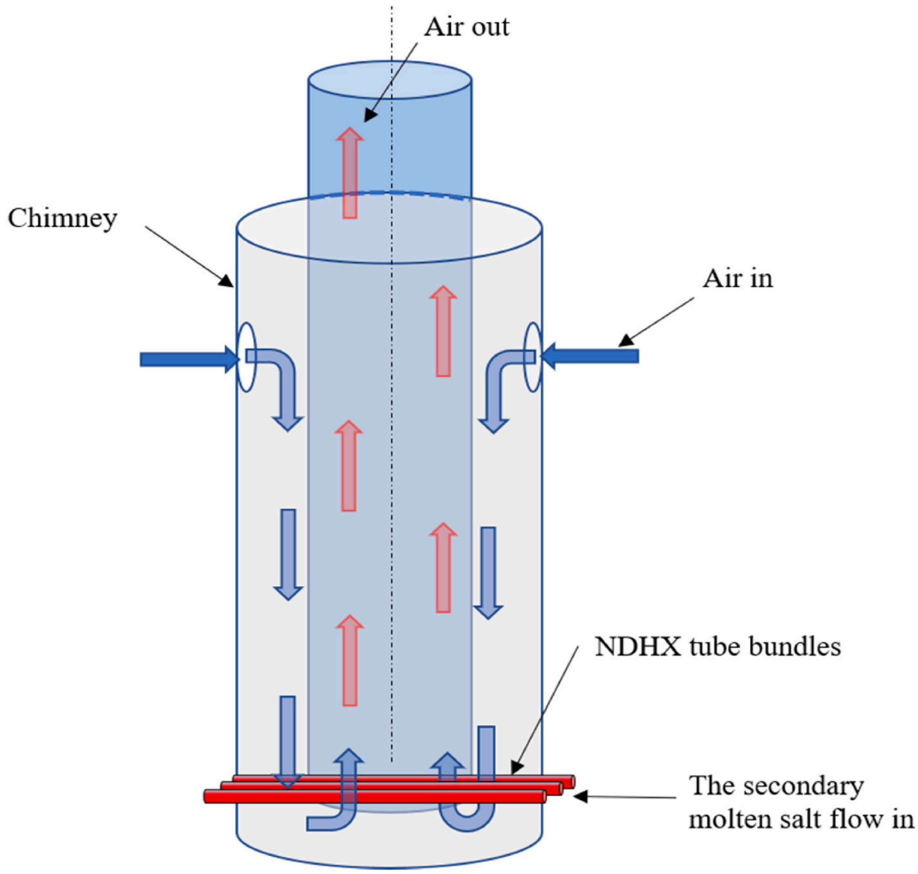

Fig. 2. Simplified schematic of an chimney with an NDHX near the bottom end [39].

2.2. Layout of novel radiative natural draft heat exchanger

A design concept is proposed herein as an alternative to the conventional NDHX design to avoid or mitigate the consequences of unexpected coolant freezing. Since the primary aim of the NDHX is to eliminate decay heat from the reactor core, thus preventing the core from overtemperature, as the fission decay continues to decrease over time, the molten salt fluid in the NDHX is gradually and inevitably cooled; once the temperature of the coolant drops to near its melting point, solidification may occur. This concern becomes increasingly critical as the melting temperature of the salt mixture adopted increases (*e.g.*, FLiNaK's melting point is 454 °C) [40].

Molten salt solidification is also intensified by the relatively high cooling efficiency of the NDHX. In addition, during a severe accident, such as a blackout, the louvres in the chimney can be kept open, and the air inflow velocity to the NDHX entirely depends on the chimney construction and cannot be decreased. In other words, the heat exchanger duty of a conventional NDHX is no longer adjustable, and undercooling of coolants can be unavoidable. To overcome this problem without relying on auxiliary heaters, external power or control, this study proposes an alternative NDHX design that relies on a passive, nonlinear variation of both the radiative and convective thermal power as the temperatures vary – as would be expected for different operation conditions.

Specifically, the primary heat transfer mechanism employed in conventional NDHX designs is convection, driven by ambient airflow over the external surface of the tube bundle that cools the heat exchanger. However, as mentioned earlier, the inlet air flow rate cannot be controlled during emergency operation, which means that the convective thermal performance in a conventional NDHX cannot be adjusted.

Thermal radiation, unlike convection, is unaffected by the external air velocity and scales with the fourth power of temperature. Thus, the possibility of emitting a significant amount of radiative heat at high temperatures and much reduced heat at low temperatures in a highly nonlinear fashion, offers an intrinsically safe way to reject heat without causing solidification and serves as a possible passive-safety characteristic that can be employed for designing advanced NDHXs in MSRs, amongst other applications.

Accordingly, the rationale of the alternative RHX design proposed here is to harness this nonlinear thermal performance by promoting thermal radiation as the primary heat transfer mechanism while suppressing the role of convection by avoiding direct contact between the external air and heat exchanger tubes of NDHX. The layout of a possible RHX design with these features is presented in Fig. 4. In this RHX design, the tubes are of the exact dimensions as those in the SHX, but they are arranged into four rows (25 tubes per bundle). Contrary to the horizontal arrangement employed in the SHX, the four rows are installed vertically. In addition, five stainless-steel plates, which are folded to achieve a zigzag 'radiant absorber' (see Fig. 4), are placed, in pairs, within the tube bundles without physically touching each other. These are used to separate the tubes from the flowing air and to absorb the radiative heat emitted from the tubes' hot surfaces. Finally, the gap between the RHX tubes and stainless-steel plates is set to be relatively small, thus limiting the internal flow.

Radiation is emitted in the RHX by the hot tubes containing the hot molten salt flow in the DRACS secondary loop and absorbed by the radiant absorbers. The radiant absorbers are then cooled down by air circulation flowing in the gap between each pair of plates. Ideal RHX performance involves removing decay heat rapidly at high-temperature conditions when the core is hot while inhibiting heat transfer passively when the core is cooled down, and the salt is susceptible to

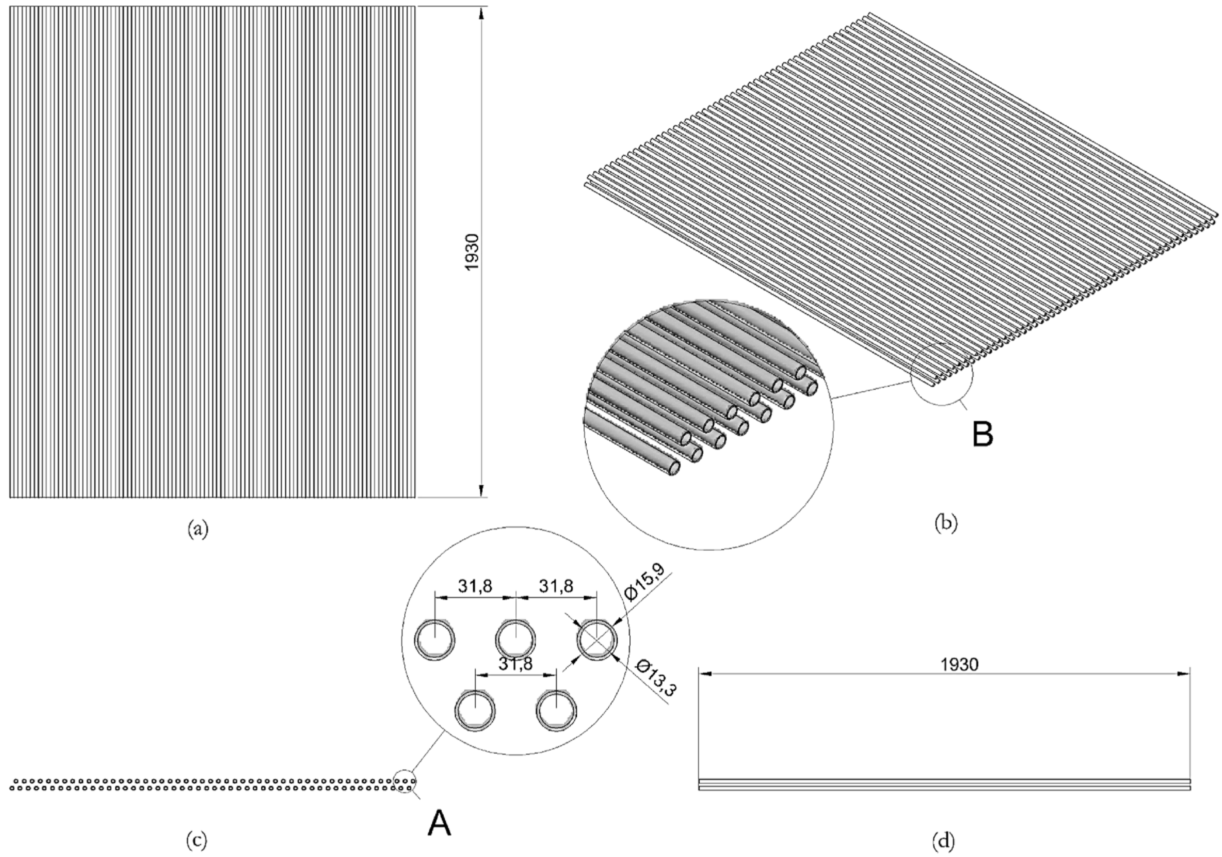

Fig. 3. Multi-view drawing of SHX: (a) top view; (b) isometric view; (c) front view; (d) side view.

solidification. For further enhancement of the thermal radiation, the external surfaces of all tubes and radiant absorbers are painted uniformly with a high emissivity coating (black). It is noted that in future, more advanced RHX designs can feature emissivity control principles to further promote radiative heat transfer at lower temperatures and suppress it at higher temperatures. This would involve using a selective coating with a high emissivity over the range of wavelengths associated with blackbody radiation at lower temperatures, and a low emissivity at wavelengths associated with blackbody radiation at higher temperatures.

3. Modelling methodology

3.1. Thermohydraulic model

To evaluate the effectiveness of the new NDHX design (RHX) and compare it against the conventional design (SHX), a thermohydraulic model was developed to simulate the operation of the heat exchanger. The thermohydraulic model employs a one-dimensional (1-D) approach to predict heat transfer. The developed model is a system of nonlinear heat transfer equations along the radial direction of the heat exchanger tube following the heat transfer and heat exchanger design approach described in Ref. [41].

The assumptions used in the model are the following: (1) the flows are fully developed, at steady-state and incompressible; (2) the temperature distribution at the axial direction is uniform, and the axial heat transfer is negligible; (3) every tube has a lumped temperature at each point in time; (4) the heat transfer coefficient to the ambient air remains constant throughout the heat exchanger's operation; and (5) thermal radiation between any two heat exchanger tubes is negligible. The set of equations comprising the model is discussed in the following sections and is divided into: (1) a set of heat transfer equations respectively for the SHX and RHX; (2) a set of equations to describe the heat transfer coefficients and physical properties; and (3) a set of equations for the decay heat. The system of equations was solved in MATLAB.

3.1.1. Heat transfer in conventional heat exchanger

In the SHX, assuming a quasi-steady state, the waste heat dissipated by the bulk of salt (Q_s) is the same as the heat transferred across the wall of the tubes (Q_w), and equal to the sum of the heat transferred by the tubes to the surrounding via the circulating air by convection (Q_{conv}); therefore:

$$Q_s = Q_w = Q_{conv} \tag{1}$$

Starting from the inside of the tube, the decay heat is transferred through the bulk of the molten salt:

$$Q_s = h_{salt} A_{w,in} \left(T_s - T_{w,in} \right) \tag{2}$$

where h_{salt} is the heat transfer coefficient of molten FLiNaK (to distinguish between the steady-state HTC h_s), $T_{w,in}$ and $A_{w,in}$ indicate, individually, the temperature and the surface area of the inside wall of the tube (in contact with the salt). The inlet temperature of coolant (T_s) is considered an input parameter.

The heat is transferred by conduction through the wall of the tube by the temperature gradient between the inside and outside temperature of the wall (T_{in} and T_{out}),

$$Q_w = \frac{\left(T_{w,in} - T_{w,out} \right)}{R} L \tag{3}$$

in which L is the axial length, and R is the thermal resistance of the tube in the radial direction:

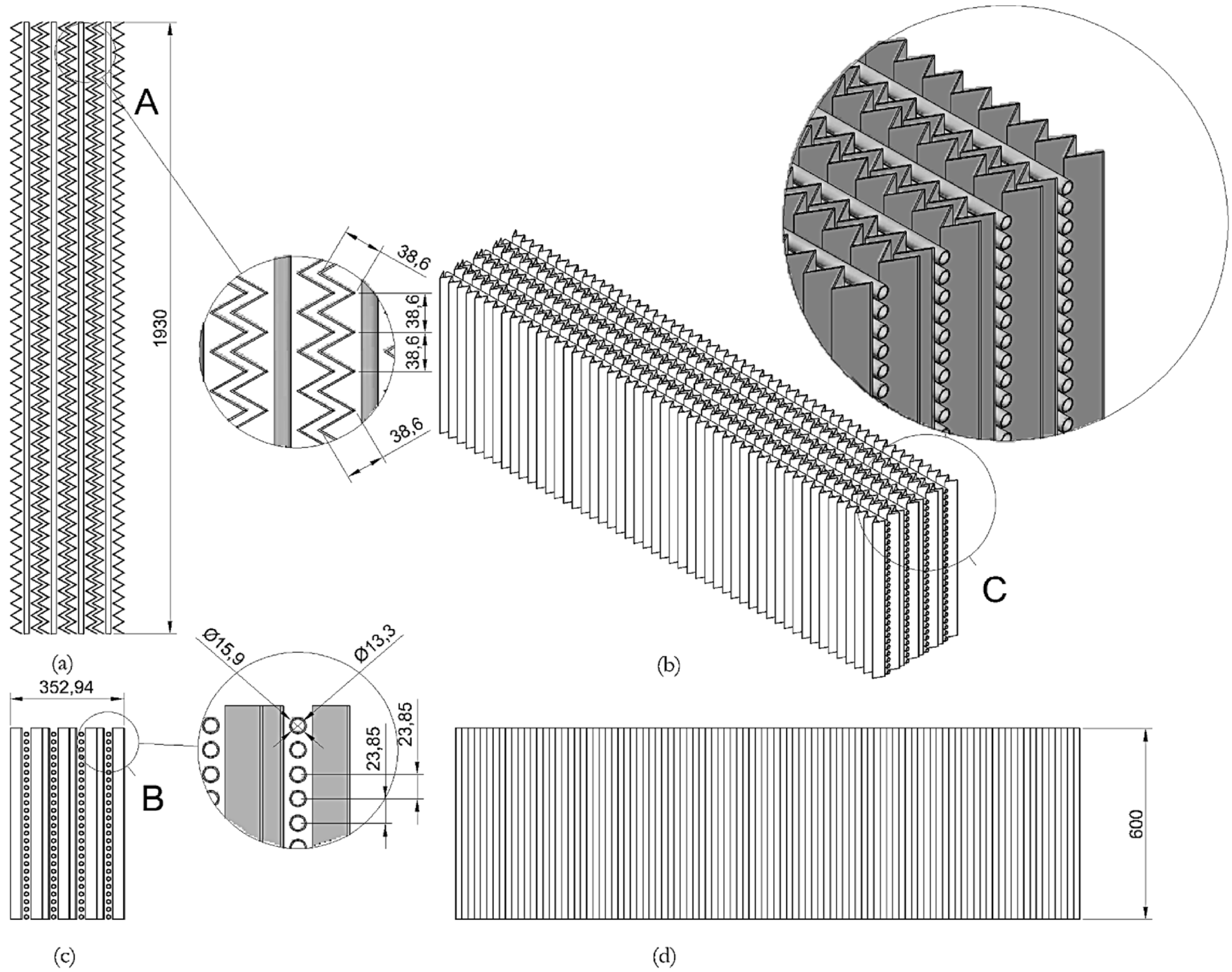

Fig. 4. Multi-view drawing of RHX concept: (a) top view, where the tubes are in grey while the radiant absorbers are visible in black; (b) isometric view; (c) front view; (d) side view.

$$R = \frac{\ln\left(\frac{r_{out}}{r_{in}}\right)}{2\pi k_w} \tag{4}$$

where k_W is the thermal conductivity of the material of the tube walls (here considered as stainless steel), and r_{in} and r_{out} represent, respectively, the inner and outer radii of the tube.

Eventually, the heat is discharged via to the ambient air in the chimney by natural convection (Q_{conv}):

$$Q_{conv} = h_s A_{w,out}\left(T_{w,out} - T_{air}\right) \tag{5}$$

where the heat transfer coefficient h_s is assumed constant and is used as a sensitivity parameter in the model, and $A_{w,out}$ is the external surface area of the tube. The subscript 'w' represents the tube wall.

3.1.2. Heat transfer in radiative heat exchanger

As opposed to the SHX, in the RHX (illustrated in Fig. 4), the external surfaces of the RHX tubes are not in direct contact with the circulating air. In this case, the heat dissipated by the tubes is equal to the radiative heat dissipated to the radiant absorber (Q_{rad}) plus the dissipation in the gap by convention (Q_{gap}), and Eq. 1 becomes:

$$Q_s = Q_w = Q_{rad} + Q_{gap} = Q_{conv} \tag{6}$$

The heat transfer equations describing Q_s, Q_w and the convective heat are eventually removed by the cooling airflow (Q_{conv}) are the same as in the previous case. The radiative heat dissipates to the absorber plates considered two-surface enclosures, where radiation (Q_{rad}) is given as:

$$Q_{rad} = \frac{\sigma\left(T_{w,out}{}^4 - T_{abs}{}^4\right)}{\frac{1-\varepsilon_w}{A_{w,out}\varepsilon_w} + \frac{1}{A_{w,out}F} + \frac{1-\varepsilon_{abs}}{A_{abs}\varepsilon_{abs}}} \tag{7}$$

where T_{abs} and A_{abs} are the surface temperature and area of the flat-side of the radiant absorber, and the view factor F is calculated by analysing the radiation between two adjacent tubes, one on top of the other (F_{adj}) [42]:

$$F_{adj} = \frac{\sqrt{\left(\frac{H}{r_{out}}\right)^2 - 4} - \frac{H}{r_{out}} + 2\arcsin\left(\frac{2}{\frac{H}{r_{out}}}\right)}{2\pi} \tag{8}$$

where H is the distance between the centres of two neighbouring tubes. The view factor between the tube and the radiant absorbers can then be calculated considering that the sum of the view factors of the two adjacent tubes and the plates must be 1. Therefore:

$$F = 1 - 2F_{adj} \tag{9}$$

3.1.3. Thermophysical properties and correlations

The system of equations is completed by knowing the values of all thermophysical properties and heat transfer coefficients. The secondary-loop coolant is FLiNaK, a fluoride salt mixture with a melting point of 454 °C and a boiling point of 1570 °C [40]. The specific heat of FLiNaK is considered constant and equal to 1880 J/kg•K [43]. The thermophysical properties of FLiNaK and air have been evaluated using the correlations below.

The thermal conductivity, density and viscosity of the salt (FLiNaK) are determined, respectively, by using relations taken from Ref. [21] and Ref. [44]:

$$k_s = 0.43 + 5.0 \times 10^{-4} T_s \tag{10}$$

$$\rho_s = 2730 - 0.73 T_s \tag{11}$$

$$\mu_s = 4.0 \times 10^{-5} \exp\left(\frac{4170}{T_s}\right) \tag{12}$$

The heat transfer coefficients were evaluated from the Nusselt number:

$$h_{salt} = \frac{Nu_s k_s}{D} \tag{13}$$

which was calculated from correlations for Newtonian pipe flow; specifically, for laminar flow ($Re < 2300$) from [45]:

$$Nu_s = 3.66 + \frac{\frac{0.0668RePrD}{L}}{1 + 0.04\left(\frac{RePrD}{L}\right)^{\frac{2}{3}}} \tag{14}$$

for transitional flow [46] ($2300 < Re < 4000$) from:

$$Nu_s = \frac{\frac{f}{8}(Re - 1000)Pr}{1.00 + 12.7\sqrt{\frac{f}{8}}\left(Pr^{\frac{2}{3}} - 1\right)} \tag{15}$$

and for turbulent flow ($Re > 10000$) from [47]:

$$Nu_s = 0.023 Re^{0.8} Pr^{0.3} \tag{16}$$

where Re is Reynold's number, Pr is Prandtl number, and f is the friction factor.

Furthermore, for flow through a straight round pipe, the friction factor f can be evaluated from [46]:

$$f = 3.03 \times 10^{-12} Re^3 - 3.67 \times 10^{-8} Re^2 + 1.46 \times 10^{-4} Re - 0.151 \tag{17}$$

The thermophysical properties of the circulating ambient air were taken from Ref. [48]. The thermal conductivity, density, dynamic viscosity and specific heat capacity were calculated using the following empirical relations:

$$k_{air} = \frac{2.33 \times 10^{-3} T_{air}^{\frac{3}{2}}}{165 + T_{air}} \tag{18}$$

$$\rho_{air} = \frac{352.0}{T_{air}} + \frac{344.8}{T_{air}^2} \tag{19}$$

$$\mu_{air} = \frac{1.46 \times 10^{-6} T_{air}^{\frac{3}{2}}}{109 + T_{air}} \tag{20}$$

$$c_{p_{air}} = 1030 - 0.20 T_{air} + 3.970 \times 10^{-4} T_{air}^2 \tag{21}$$

The convective heat transfer within the gap between the bundle of tubes and the radiant absorbers was calculated using the empirical correlation [49] for natural convection:

$$Nu_{air} = 0.579\left(\frac{GrPr}{\left[1 + (0.442/Pr)^{\frac{9}{16}}\right]^{\frac{16}{9}}}\right)^{\frac{1}{4}} \tag{22}$$

where Gr is the Grashof number which is defined as:

$$Gr = \frac{g\beta T_{air} D^3}{\mu^2} \tag{23}$$

and the temperature of the air used to calculate the thermophysical properties is taken as an average between the temperature of the tube and the absorber plate. As mentioned above, the heat transfer coefficient on the air-side, h_s, is used here as a sensitivity parameter.

3.1.4. Decay heat generation

The decay heat generated in a fission reactor after an emergency shutdown can be calculated by knowing the type of fuel, the concentration of fission products, and the half-lives of those products [50]. By using the Wigner-Way formula, the decay generation over time ($P_d(t)$) can be estimated from:

$$P_d(t) = 0.0622 P_0 \left[t^{-0.2} - \left((t_0 + t)^{-0.2}\right]\right. \tag{24}$$

where P_0 is the reactor thermal power before the scram and t_0 the power history of the reactor. In the present study, the thermal capacity of the MSR before shutdown was taken as 20 MW considering a 6-month power history with 0.2 MW decay rate following the same prototypical reactor as in Ref. [21].

3.2. Sensitivity analysis

A sensitivity analysis was applied to determine how changes to the independent variables can influence the solidification of the coolant and the heat transfer performance of the heat exchanger. In total, two separate scenarios are simulated using the thermohydraulic model by varying: (1) the bulk temperature of the salt in the tubes (T_s); and (2) the steady-state air-side heat transfer coefficient (h_s) in the NDHX. These two scenarios simulate the operation of the NDHX over various temperature ranges, unexpected cooling events, and strong or weak natural circulation in the chimney. Specifically, the bulk temperature of the salt varied in the range of 450–1100 °C. A temperature of 1100 °C was purposely estimated to be the highest temperature of molten salts in the secondary loop that is still within safety limitations [33]. After a scram event, the temperature of the salt entering the NDHX decreases over time as the reactor decay heat decreases. The nominal steady-state air-side heat transfer coefficient was varied between 35 W/(m^2•K) (from Ref. [39]) and 60 W/(m^2•K), assuming a more extreme operating situation with respect to solidification.

Three quantities are employed to evaluate the performance of both NDHX designs under various scenarios mentioned above: (1) heat duty (*e.g.*, heat rejection/removal rate) of both heat exchangers, evaluating their heat removal performance; (2) temperature at the inside/internal wall of the tube (in contact with the molten salt), as suggested in Ref. [21], which is used as a conservative criterion to evaluate the feasibility of a NDHX design; and (3) time before the molten salt temperature drops below its melting point after a scram event, which is used to quantify the capability of both heat exchangers to delay the phenomenon of molten salt solidification.

4. Results and discussion

4.1. Performance at different molten salt inlet temperatures

To compare their performance, heat duty (Q) was evaluated for both SHX and RHX under various inlet temperatures. These quantities are shown in Fig. 5 for a nominal case where the air-side heat transfer coefficient is 35 W/m^2•K. Considering quasi-steady state operation in the DRACS circuit, the inlet temperature of the salt reaches an equilibrium temperature such that the heat transferred to the airflow equals the decay heat from the reactor. By calculating this heat at different inlet salt temperatures, we can obtain the dotted blue and dashed red lines in

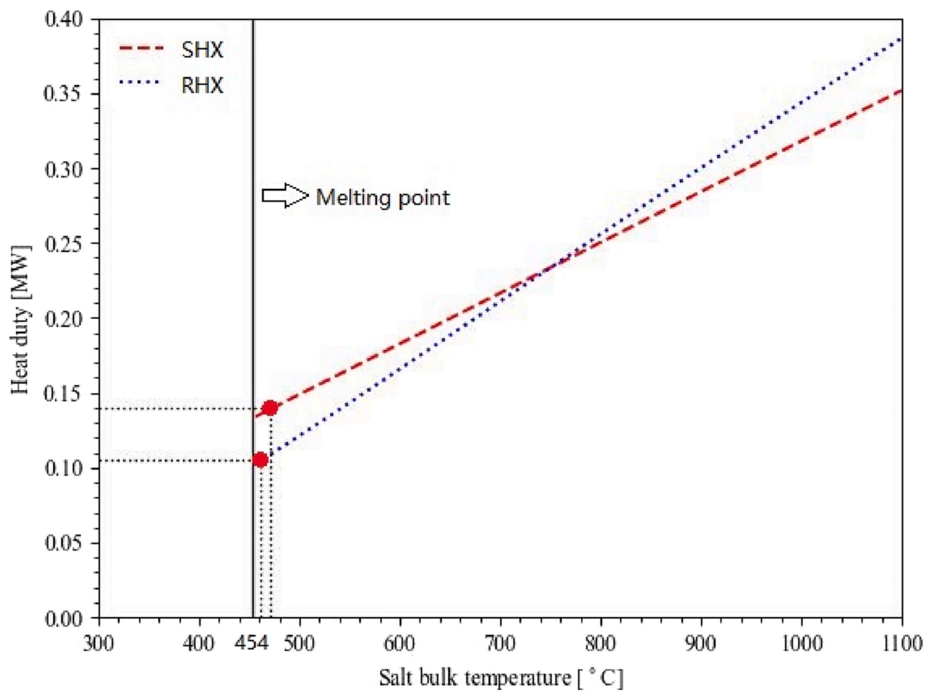

Fig. 5. Heat exchanger duties for different NDHX designs (Q), both SHX and RHX, as predicted by the thermodynamic model by varying the inlet temperature of the molten salt (T_s), where the vertical line indicates the melting point of the fluoride salt mixture (FLiNaK).

Fig. 5 for the SHX and RHX, respectively.

As shown in the figure, the RHX line has a steeper slope than that of the SHX, with lower heat duties at lower temperatures and higher heat duties at higher temperatures, as intended. This arises from the different operating modes of the RHX, with radiative heat transfer dominating overall and being significantly reduced at low temperatures, thus making the RHX less thermally effective than the SHX under these conditions. However, at higher temperatures, the contrary holds true, with the RHX performing better than the SHX thanks to its larger contact area with the airflow (11.8 m^2 vs 9.9 m^2 of SHX). The larger area of the RHX (compared to the SHX) is a direct result of the sizing conducted to achieve a nominal heat duty of 0.2 MW in both heat exchangers, *i.e.*, in order to achieve the same duty at the design condition, the RHX, with the added heat transfer resistances caused by the gap between the tubes and the heat absorption plates, had to be larger than the SHX. The larger area, in turn, increases the safety range of operation of the RHX at higher temperatures. Indeed if 1100 °C is taken as the temperature above which the salt becomes unstable, the RHX (and therefore DRACS) can handle 0.39 MW of decay heat. In contrast, the SHX can sustain only 0.35 MW, an improvement of over 10 %.

The red dots in Fig. 5 indicate the onset of salt solidification inside the heat exchanger or the point below which it is not safe to operate the unit. This temperature is taken as the inlet salt temperature, which would make the temperature of the inner wall of the tubes fall below the melting point of the salt. This temperature is lower for the RHX due to the fact that it has a higher wall temperature than the SHX. More importantly, the heat necessary to cause the onset of solidification is around 0.14 MW for the SHX and 0.10 MW for the RHX, representing a close to 30 % decrease. Overall, the range of decay heats that the RHX can safely manage (without causing the onset of solidification) is from 0.10 MW to 0.39 MW compared to the 0.14 MW to 0.35 MW range of the SHX, which corresponds to an increase of almost 40 %.

Another NDHX performance evaluation criterion is the time before the first solidification occurs after a scram. We can calculate this time assuming quasi-state conditions in the DRACS. This assumption holds true as long as the timescale to thermally equilibrate the DRACS loops is much shorter than the timescale of decay heat decrease. The timeframe to thermally equilibrate DRACS given a drop of decay heat (say 0.05 MW, from 0.2 MW to 0.15 MW) is of the order of 300 s (considering the time to heat up around 500 kg of salt present in the DRACS loops). The amount of decay heat being generated in a fuel assembly after scram can be precisely measured once the type of fuel, concentrations of fission products, decay energies and half-lives of those products are known [50]. It is also possible to give a rough approximation by the Wigner-Way formula [44]. In the present study, the thermal power of the MSR before the shutdown was assumed to be 20 MW with a power history of 6 months. Then the approximation of decay power is sketched in Fig. 6. As it can be seen from Fig. 6, at 0.2 MW of reactor power, the timescale to decrease by 0.05 MW is much longer, and the assumption holds true.

Considering the assumption mentioned above, we can calculate the time it would take for the DRACS to reach unsafe operation (red points in Fig. 5) from the decay heat curve (Fig. 6). In more detail, we can estimate from the Wigner-Way formula the time needed for the decay heat to reach the minimal heat duties, respectively, for the SHX and the RHX. The simulation results indicated above show that these minimal heat exchanger duties of RHX and SHX are 0.09 MW (0.45 % of the core power) and 0.12 MW (0.6 % of the core power). Based on Fig. 6, the decay rate reaches the minimum heat duty of the SHX (red dot) after 3.8 h; however, the RHX design takes approximately 10.8 h to reach the minimal heat duty, which is promising and strong evidence that the RHX can mitigate issues and risks associated with coolant solidification.

4.2. Performance for different heat transfer coefficients

In this second assessment scenario, we conducted simulations by varying the value of the steady-state, air-side heat transfer coefficient (h_s) in the NDHXs. This value is critical to the performance of the NDHX and needs to be maintained within a safe range. A value of the heat transfer coefficient that is too low will result in an inability of the DRACS to dissipate the decay heat. In contrast, an over-conservative design approach resulting in a heat transfer coefficient that is too higher will increase the likelihood of solidification. By varying the heat transfer coefficient, we can calculate the maximum and minimum heat duties that the NDHX can handle without reaching unsafe operation, which

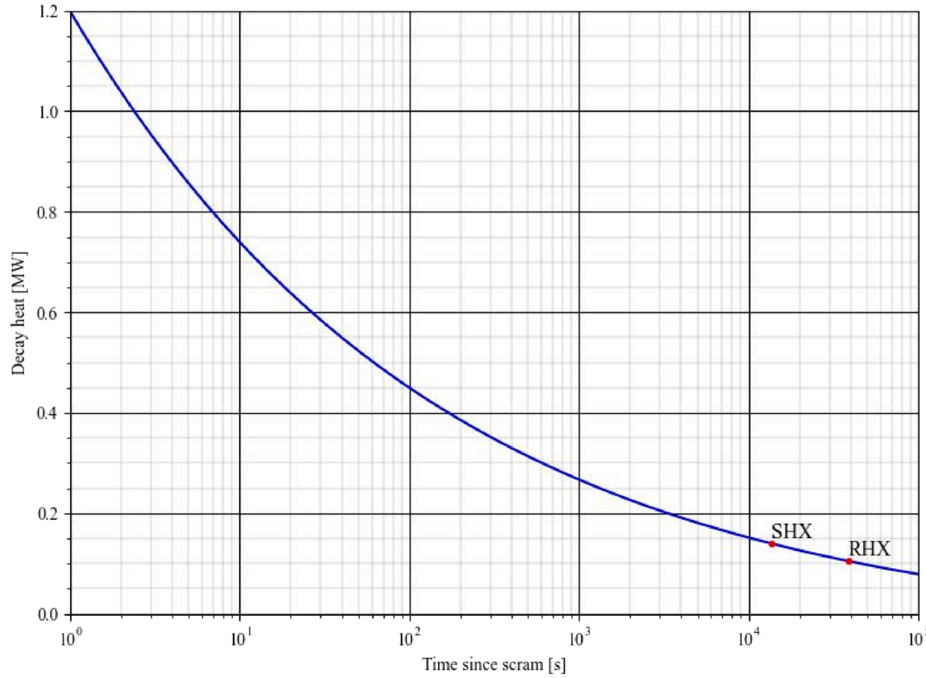

Fig. 6. Decay heat generation over time in a newly shutdown reactor, which is assumed to operate at a power of 20 MW with a 6-month power history. The red dots represent the time saved by each NDHX design before the first solidification might occur and correspond to approximately 6.3 hr and 18 hr for the SHX and RHX, respectively. (For interpretation of the references to colour in this figure legend, the reader is referred to the web version of this article.)

are: (1) an inner tube wall temperature which is less than the solidification temperature of the salt (hereby taken as 454 °C); and (2) a bulk temperature of the salt which is higher than the stability temperature of the salt (hereby taken as 1100 °C).

Fig. 7 and Fig. 8 show, respectively, operational maps of the SHX and RHX designs as derived by calculating the maximum and minimum allowable duties, as explained above. The green area is where operation is considered safe. As shown, the safe operating area of the RHX is significantly larger than the SHX. The performance of the RHX is especially better for higher values of the air-side heat transfer coefficient, meaning that the risk involved with the potential underestimation of such a heat-transfer coefficient is much more mitigated. This is

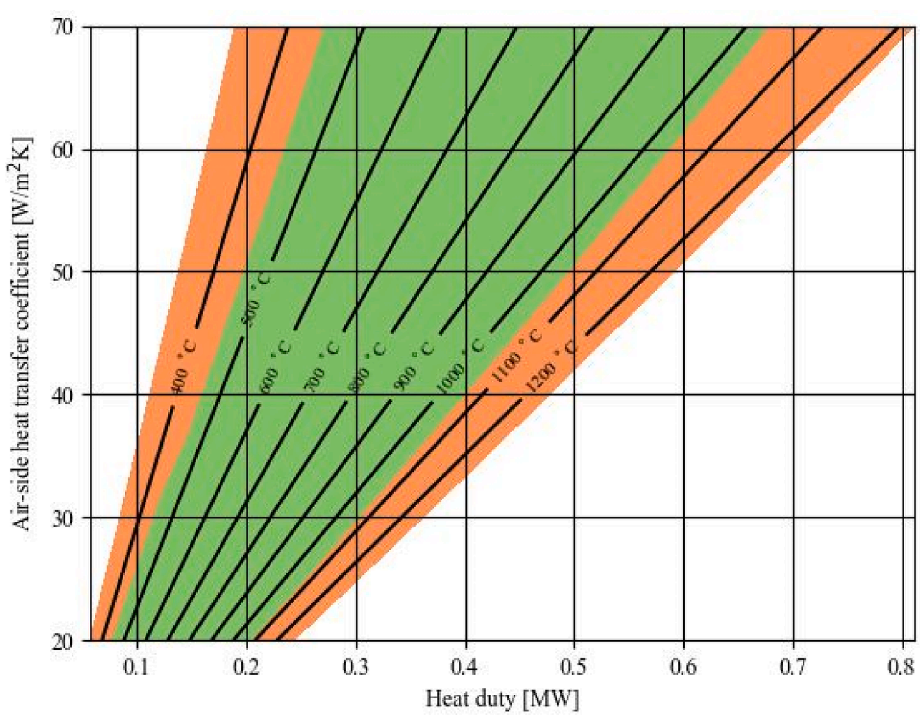

Fig. 7. Operational map of SHX as a function of the heat duty of the NDHX and air-side heat transfer coefficient. Green area: operation is considered safe, preventing salt instability and solidification. Orange area: operation is considered unsafe but still feasible. Black lines: temperature of the inner-tube wall. (For interpretation of the references to colour in this figure legend, the reader is referred to the web version of this article.)

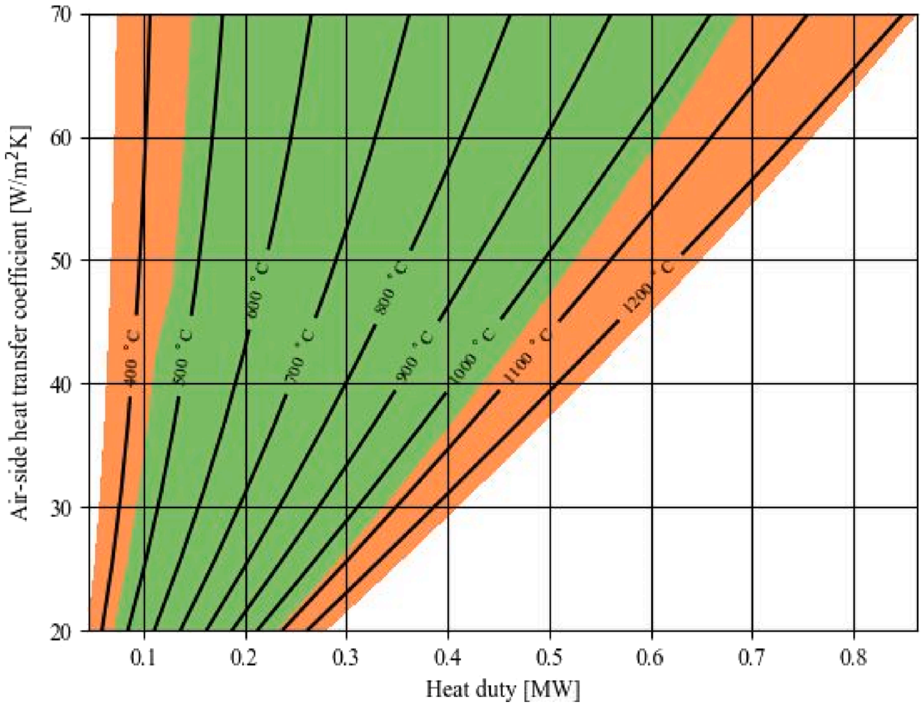

Fig. 8. Operational map of the RHX as a function of the heat exchanger heat duty and air-side heat transfer coefficient. Green area: operation is safe, preventing salt instability and solidification. Orange area: operation is unsafe but still feasible. Black lines: temperature of the inner-tube wall. (For interpretation of the references to colour in this figure legend, the reader is referred to the web version of this article.)

especially relevant if fins or other means of heat-transfer enhancement are used to increase the heat rejection capabilities so that the DRACS can cope with higher values of decay heat. The figures also show the temperature of the inner wall, which increases with a higher heat duty and a lower air-side heat transfer coefficient. As expected, the wall temperature of the RHX is higher than the SHX due to the higher heat transfer resistance caused by the absorption plates.

5. Conclusions

This paper presented an innovative approach for designing heat exchangers for applications requiring specific characteristics. It examined, as an exemplary case study, the problems associated with using high-melting temperature molten salt mixtures as heat transfer fluids (HTFs) in risk-prone applications, specifically by alleviating molten salt solidification. As part of this effort, the paper investigated the propensity for molten salt solidification in the natural draft heat exchanger (NDHX). This air-cooled heat exchanger is considered the most vulnerable component in terms of its susceptibility to coolant solidification in the direct reactor auxiliary cooling system (DRACS), which is a passive safety cooling system for molten salt reactors (MSRs).

In this regard, an innovative approach for heat exchanger design was proposed, which promotes thermal radiation as the primary heat transfer mode, while suppressing the influence of convection. Based this approach, an alternative design of the natural draft heat exchanger referred to as a ‘radiative heat exchanger’ (RHX), was developed. By promoting thermal radiation and suppressing convective heat transfer, the RHX exploits the inherent and strongly nonlinear heat transfer properties of radiation, *i.e.*, emitting a significant amount of heat at high temperatures, while having much-reduced heat transfer rates at low temperatures. In this way, the design of the RHX can passively reduce the heat rejection/removal rates when the coolant temperature drops and is near its melting point, while promoting safe operation when excess heat needs to be removed from MSRs. To the best knowledge of the authors, this is the first time that such an approach has been used for the design of heat exchangers to address molten salt solidification. Such operation characteristics pave the way for designing heat exchangers that do not rely on external power or control to avoid coolant solidification.

A thermohydraulic model was developed to simulate heat transfer in such a heat exchanger. The model was developed in one dimension under a steady-state assumption. The bulk temperature of the coolant was employed as the primary dependent variable to evaluate the risk of coolant solidification (via comparisons to the salt’s melting point). The model was then applied to evaluate the thermal operation and heat transfer performance of the RHX and to compare this to a conventional NDHX. A sensitivity analysis was conducted over their operating envelopes.

Based on the results of the model, it can be concluded that the new design provides nonlinear thermal-energy removal performance that can self-regulate based on the needs of the reactor core without any external controls (manual or automatic). For the case study in the present paper, it was shown that in the case of a prototypical 20 MW reactor with a decay rate of 0.2 MW, the RHX has the potential to reduce the heat removal rate by approximately 30 % compared to a conventional NDHX at low temperatures. Due to this 30 % reduction in heat removal, the first instance of molten salt solidification can be delayed by 2.8 times. Specifically, the new design is capable of keeping the DRACS operating without external intervention for 10.8 h as opposed to 3.8 h when using the conventional NDHX design after a shutdown of the prototypical MSR. Additionally, the calculated heat exchanger duty is increased by 17 % when the molten salt is in the high-temperature regime compared to the conventional design. As an additional advantage of the new design, the RHX also shows robustness against the overdesign of the natural draft heat exchanger with air-side heat transfer coefficients above their rated values. The modelling results demonstrate that the RHX has the potential to sustain much higher air-side heat transfer coefficient values than the traditional natural draft heat exchanger.

Although a nuclear application was used as a case study in this specific work to demonstrate the effectiveness of the proposed heat exchanger design approach, the same principles can be applied to other applications with similar challenges or desired characterises. More advanced designs can incorporate emissivity control principles to further promote radiative heat transfer at lower temperatures and suppress it at higher temperatures. It would be desirable to utilise selective coatings with a high emissivity over the range of wavelengths associated with blackbody radiation at low temperatures and a low emissivity over the range of wavelengths associated with blackbody radiation at higher temperatures.

Declaration of Competing Interest

The authors declare that they have no known competing financial interests or personal relationships that could have appeared to influence the work reported in this paper.

Data availability

Data will be made available on request.

Acknowledgements

This work was supported by the UK Engineering and Physical Sciences Research Council (EPSRC) [grant numbers EP/R045518/1, and EP/S032622/1]. Data supporting this publication can be obtained on request from cep-lab@imperial.ac.uk. For the purpose of Open Access, the authors have applied a CC BY public copyright licence to any Author Accepted Manuscript version arising from this submission.

References

[1] A.M. Pantaleo, S.M. Camporeale, A. Miliozzi, V. Russo, N. Shah, C.N. Markides, Novel hybrid CSP-biomass CHP for flexible generation: Thermo-economic analysis and profitability assessment, Appl. Energy 204 (2017) 994–1006.
[2] A.M. Pantaleo, S.M. Camporeale, A. Sorrentino, A. Miliozzi, N. Shah, C. N. Markides, Hybrid solar-biomass combined Brayton/organic Rankine-cycle plants integrated with thermal storage: Techno-economic feasibility in selected Mediterranean areas, Renew. Energy 147 (2020) 2913–2931.
[3] M. Roeb, M. Neises, N. Monnerie, C. Sattler, R. Pitz-Paal, Technologies and trends in solar power and fuels, Energy Environ. Sci. 4 (7) (2011) 2503–2511.
[4] P. Romanos, A.A. Al Kindi, A.M. Pantaleo, C.N. Markides, Flexible nuclear plants with thermal energy storage and secondary power cycles: Virtual power plant integration in a UK energy system case study, Electron. Energy 2 (2022), 100027.
[5] M. Liu, W. Saman, F. Bruno, Review on storage materials and thermal performance enhancement techniques for high temperature phase change thermal storage systems, Renew. Sustain. Energy Rev. 16 (4) (2012) 2118–2132.
[6] N. Le Brun, C.N. Markides, A Galinstan-filled capillary probe for thermal conductivity measurements and its application to molten eutectic KNO_3–$NaNO_3$–NO_2 (HTS) up to 700 K, Int. J. Thermophys. 36 (10–11) (2015) 3222–3238.
[7] G. Bovesecchi, P. Coppa, S. Pistacchio, A new thermal conductivity probe for high temperature tests for the characterisation of molten salts, Rev. Sci. Instrum. 89 (5) (2018), 055107.
[8] Q.G. Zhao, S.J. Liu, H. Guo, X. Chen, A theoretical model for predicting the thermal conductivity of binary molten salts, Int. J. Heat Mass Transf. 92 (2016) 639–642.
[9] R. Serrano-López, J. Fradera, S. Cuesta-López, Molten salts database for energy applications, Chem. Eng. Process. Process Intensif. 73 (2013) 87–102.
[10] C. Odenthal, F. Klasing, T. Bauer, Demonstrating cost effective thermal energy storage in molten salts: DLR's TESIS test facility, Energy Procedia 135 (2017) 14–22.
[11] C. Denbow, N. Le Brun, N. Mac Dowell, N. Shah, C.N. Markides, The potential impact of Molten Salt Reactors on the UK electricity grid, J. Clean. Prod. 276 (2020) 122873.
[12] D. Kearney, et al., Assessment of a molten salt heat transfer fluid in a parabolic trough solar field, J. Sol. Energy Eng. 125 (2) (2003) 170–176.
[13] C. Wyman, J. Castle, F. Kreith, A review of collector and energy storage technology for intermediate temperature applications, Sol. Energy 24 (6) (1980) 517–540.
[14] S.M. Hasnain, Review on sustainable thermal energy storage technologies, Part I: heat storage materials and techniques, Energy Convers. Manag. 39 (11) (1998) 1127–1138.
[15] A.A. Al Kindi, M. Aunedi, A.M. Pantaleo, G. Strbac, C.N. Markides, Thermo-economic assessment of flexible nuclear power plants in future low-carbon electricity systems: Role of thermal energy storage, Energy Convers. Manag. 258 (2022), 115484.
[16] E.S. Bettis, R.W. Schroeder, G.A. Cristy, H.W. Savage, R.G. Affel, L.F. Hemphill, The aircraft reactor experiment—design and construction, Nucl. Sci. Eng. 2 (6) (1957) 804–825.
[17] J.M. Wild, Nuclear propulsion for aircraft, Astronaut. Aeronaut. 6 (1968) 24–30.
[18] R.C. Robertson, MSRE Design and Operations Report Part I Description of Reactor Design, Oak Ridge National Laboratory, TN (United States), Jan. 1965.
[19] H.G. MacPherson, The molten salt reactor adventure, Nucl. Sci. Eng. 90 (4) (1985) 374–380.
[20] J. Smith, W.E. Simmons, An Assessment of a 2500 MWe Molten Chloride Salt Fast Reactor, Atomic Energy Authority, United Kingdom, 1974.
[21] N. Le Brun, G.F. Hewitt, C.N. Markides, Transient freezing of molten salts in pipe-flow systems: Application to the direct reactor auxiliary cooling system (DRACS), Appl. Energy 186 (1) (2017) 56–67.
[22] J. Serp, et al., The molten salt reactor (MSR) in generation IV: Overview and perspectives, Prog. Nucl. Energy 77 (2014) 308–319.
[23] P. Sabharwall. Feasibility Study of Secondary Heat Exchanger Concepts for the Advanced High Temperature Reactor, Idaho National Laboratory, ID (United States), 2011.
[24] L.C. Olson, J.W. Ambrosek, K. Sridharan, M.H. Anderson, T.R. Allen, Materials corrosion in molten LiF–NaF–KF salt, J. Fluor. Chem. 130 (1) (2009) 67–73.
[25] W. Zhong, Z. Tong, G. Ning, C. Zhang, H. Lin, W. Yang, The fatigue behavior of irradiated reactor pressure vessel steel, Eng. Fail. Anal. 82 (2017) 840–847.
[26] T. Allen, J. Busby, M. Meyer, D. Petti, Materials challenges for nuclear systems, Mater. Today 13 (12) (2010) 14–23.
[27] J.C. Gomez-Vidal, R. Tirawat, Corrosion of alloys in a chloride molten salt (NaCl-LiCl) for solar thermal technologies, Sol. Energy Mater. Sol. Cells 157 (2016) 234–244.
[28] J.E. Pacheco, S.R. Dunkin. Assessment of molten-salt solar central-receiver freeze-up and recovery events, Sandia National Laboratory, CA (United States), 1996.
[29] Z. Li, Q. Zhang, Z. Wang, J. Li, Y. Ruan, Numerical and experimental study of solidification dangers in a molten salt receiver for cloudy conditions, Sol. Energy 193 (2019) 118–131.
[30] T. Abram, S. Ion, Generation-IV nuclear power: A review of the state of the science, Energy Policy 36 (12) (2008) 4323–4330.
[31] V. Voulgaropoulos, N. Le Brun, A. Charogiannis, C.N. Markides, Transient freezing of water between two parallel plates: A combined experimental and modelling study, Int. J. Heat Mass Transf. 153 (2020), 119596.
[32] C. Forsberg, et al., Fluoride-salt-cooled high-temperature reactor (FHR) using British advanced gas-cooled reactor (AGR) refueling technology and decay heat removal systems that prevent salt freezing, Nucl. Technol. 205 (9) (2019) 1127–1142.
[33] R.C. Robertson, MSRE design and operations report, I. Description of reactor design, Oak Ridge National Laboratory, TN (United States), 1965.
[34] C. Prieto, R. Osuna, A.I. Fernández, L.F. Cabeza, Thermal storage in a MW scale. Molten salt solar thermal pilot facility: Plant description and commissioning experiences, Renew. Energy 99 (2016) 852–866.
[35] National Research Council (U.S.). Committee on Lessons Learned from the Fukushima Nuclear Accident for Improving Safety and Security of U.S. Nuclear Plants, Lessons learned from the Fukushima nuclear accident for improving safety of U.S. nuclear plants.
[36] Q. Lv, et al., DRACS thermal performance evaluation for FHR, Ann. Nucl. Energy 77 (2015) 115–128.
[37] N. Le Brun, A. Charogiannis, G.F. Hewitt, C.N. Markides, Tackling Coolant Freezing in Generation-IV Molten Salt Reactors, Int. Conf. Nucl. Eng. Proceedings, ICONE 9 (2017).
[38] N. Le Brun, C.N. Markides, A Transient Model for Simulating the Freezing Process of Molten-salt Coolants, MATEC Web Conf. 68 (2016).
[39] Q. Lv, X. Sun, R. Chtistensen, T. Blue, G. Yoder, D. Wilson, Design, testing and modeling of the direct reactor auxiliary cooling system for AHTRs, Oak Ridge National Laboratory, TN (United States), 2015.
[40] D.F. Williams, Assessment of candidate molten salt coolants for the NGNP/NHI heat-transfer loop, Oak Ridge National Laboratory, TN (United States), 2006.
[41] S.P. Venkateshan, Heat Transfer, Springer, 2021.
[42] J.R. Howell, M.P. Mengüç, Radiative transfer configuration factor catalog: A listing of relations for common geometries, J. Quant. Spectrosc. Radiat. Transf. 112 (5) (2011) 910–912.
[43] D.J. Rogers, T. Yoko, G.J. Janz, Fusion properties and heat capacities of the eutectic lithium fluoride-sodium fluoride-potassium fluoride melt, J. Chem. Eng. Data 27 (3) (1982) 366–367.
[44] M. Arkani, M. Gharib, Residual heat estimation by using Cherenkov radiation in Tehran Research Reactor, Nucl. Instrum. Methods Phys. Res. Sect. A Accel. Spectrometers, Detect. Assoc. Equip. 596 (3) (2008) 417–421.
[45] F.P. Incropera, Fundamentals of Heat and Mass Transfer, John Wiley, 2007.
[46] J.P. Abraham, E.M. Sparrow, W.J. Minkowycz, Internal-flow Nusselt numbers for the low-Reynolds-number end of the laminar-to-turbulent transition regime, Int. J. Heat Mass Transf. 54 (1–3) (2011) 584–588.
[47] F.W. Dittus, L.M.K. Boelter, Heat transfer in automobile radiators of the tubular type, Int. Commun. Heat Mass Transf. 12 (1) (1985) 3–22.
[48] F.J. McQuillan, J.R. Culham, M.M. Yovanovich. Properties of dry air at one atmosphere, Microelectronics Heat Transfer Lab, University of Waterloo, ON (Canada), June 1984.
[49] S.K.S. Boetcher, Natural Convection Heat Transfer from Horizontal Cylinders, in: SpringerBriefs in Applied Sciences and Technology, Springer, 2014.
[50] B.J. Ade, I.C. Gauld, Decay heat calculations for PWR and BWR assemblies fueled with uranium and plutonium mixed oxide fuel using SCALE, Oak Ridge National Laboratory, TN (United States), 2011.